TELKOMNIKA Telecommunication Computing Electronics and Control
Vol. 24, No. 2, April 2026, pp. 387~395
ISSN: 1693-6930, DOI: 10.12928/TELKOMNIKA.v24i2.27564

Dual-band performance enhancement of terahertz patch antennas via slotting method

Bich Ngoc Tran-Thi, Trong Hai Le
Department of Air Traffic Management Technical System, Faculty of Aviation Operations, Vietnam Aviation Academy, Ho Chi Minh City, Vietnam

Article Info

Article history:

Received Sep 22, 2025
Revised Dec 12, 2025
Accepted Jan 30, 2026

Keywords:

Dual-band terahertz
Patch antenna
Return loss
Sixth-generation
Voltage standing wave ratio

ABSTRACT

Sixth-generation (6G) wireless networks are designed to provide ultra-high data rates with latencies as low as one microsecond, operating at frequencies higher than those used in fifth-generation (5G) networks. This study focuses on a compact and flexible dual-band terahertz (THz) rectangular patch antenna utilizing a slot cutting technique. The antenna features strategically placed rectangular slots on its patch, with dimensions of 1×1×0.1 mm. Its performance was simulated using computer simulation technology (CST) Studio Suite simulation software. The results indicate that the antenna operates at frequencies of 147.42 GHz and 202.5 GHz, achieving gains of 2.66 dB and 4.52 dB, respectively. Notably, the designed antenna demonstrates excellent impedance matching, as evidenced by deep return loss values of −19.818 dB and −44.776 dB. Furthermore, the findings report a voltage standing wave ratio (VSWR) of 1.01. This antenna design is suitable for applications in aerospace, 5G handheld devices, wireless communication, and THz medical imaging.

Corresponding Author:

Bich Ngoc Tran-Thi
Department of Air Traffic Management Technical System, Faculty of Aviation Operations
Vietnam Aviation Academy
Ho Chi Minh City, Vietnam
Email: ngocttb@vaa.edu.vn

1. INTRODUCTION

The rapid growth of wireless communication has led to a significant increase in data transmission demands. As the number of mobile and wireless devices increases, the limitations of current bandwidth and latency become more apparent. Sixth-generation (6G) wireless technology represents a major advancement beyond 5G, providing reliable connectivity in a variety of environments, minimal latency, and much faster data rates. According to industry forecasts, data rates may exceed gigabits per second (Gbps) and approach terabits per second (Tbps) within the next decade [1]. To meet these criteria, 6G networks are projected to use the terahertz (THz) frequency range, which ranges approximately from 0.1 to 10 THz, and delivers extensive bandwidth with very low latency [2]. One of the key objectives is to achieve a latency as low as one microsecond [3], [4]. Due to its unique properties, the THz band makes it suitable for a wide range of applications, including biological systems [5], [6], imaging [7], [8], wireless communication [9], [10], and spectroscopy [11], [12], with significant potential in aerospace communication and autonomous flight control. However, it also faces notable challenges, such as high signal attenuation and path loss caused by water vapor and molecular absorption in the atmosphere [13].

Antennas are essential components of wireless communication systems, acting as a link between electromagnetic waves and electronic circuits. They are necessary for signal transmission and reception,

thereby influencing the overall efficiency and reliability of the system. In 6G networks, antenna design must adapt to support effectively at higher frequency bands, including millimeter-wave (mmWave) and THz ranges, where wavelengths are considerably shorter. This transition requires antennas with reduced physical dimensions, high radiation efficiency, enhanced directivity, and advanced beamforming capabilities to ensure reliable signal transmission and reception in complex environments, effectively addressing increased path loss and atmospheric absorption [4]. For 6G applications operating in the THz frequency band, antenna design must meet several critical specifications [4], [14]:

- Frequency range: THz band (0.1–10 THz) is essential for ultra-high-speed data transmission.
- Bandwidth: ultra-wideband (UWB) and multi-band antennas are required, with fractional bandwidths exceeding 50%, to support high data rates and multiple use cases.
- Radiation pattern: depending on the application, both omnidirectional and highly directional antennas are needed.
- Size and cost: compact and low-cost designs are preferred to facilitate integration and mass deployment.
- Polarization: circular polarization is advantageous for reducing polarization mismatch and improving signal robustness.
- Functionality: multi-band antennas enhance system capacity and flexibility, enabling multi-purpose use across different scenarios.

Depending on the antenna design's purpose, various techniques, shapes, or materials are applied to achieve the desired outcome. Krishna Ch *et al*. [15] proposed a compact graphene-based microstrip patch antenna operating in the THz range, featuring a modified E-shaped patch with a slot-loaded T-shaped ground plane. With dimensions of only 130×100 μm², it achieves a maximum reflection coefficient of −19.49 dB at a resonant frequency between 0.57 and 1.02 THz. By utilizing this shape, the design improves the fractional bandwidth by approximately 892.98% compared to the conventional baseline. The peak radiation efficiency is nearly 92%. Another way to enhance antenna features is with a fractal butterfly antenna [16], built from independent fractal unit groups. The design improves coupling and reduces loss compared to a traditional butterfly antenna-showing −33.59 dB return loss and about 85%−10 dB bandwidth at 4.9 THz and achieves roughly 0.945 absorption efficiency. Additionally, this antenna operates across 0.1–10 THz with an approximately 85% −10 dB impedance bandwidth at 4.9 THz, a minimum return loss near −33.59 dB, and a maximum gain around 16.95 dB. Aqlan *et al*. [17] presented a compact conical horn antenna, integrated with a circular polarizer disk and WR-03 waveguide feed, resonating at 312 GHz. It achieved a minimum axial ratio of 1.15 dB and maintains S11 below −15 dB over the 270–330 GHz band. Another approach to enhancing the antenna's characteristics is discussed in [18]. The proposed lens-based antenna, powered by a G-band leaky-wave source and equipped with a dielectric grid polarizer, operated at over 100 GHz with a 44% relative bandwidth. When utilized with a focal plane array, it had an axial ratio of less than 3 dB over 35% bandwidth, an aperture efficiency of more than 75%, and the ability to sustain multiple directional circularly polarized beams. The circularly polarized dielectric lens antenna is introduced in [19], composed of variable-height dielectric posts and a bottom grating, which converts linearly polarized input into circularly polarized output. Fed by a standard pyramidal horn, it operated at 300 GHz with a peak gain of 30.8 dB. To further enable tri-band operation for THz applications in a compact form factor, the author in [20] added rectangular and semicircular slots to the radiating patch. This patch, made of polyimide with copper, measures about 1.4×1.1×0.14 mm³. It works at three frequencies: 123 GHz, 168 GHz, and 182 GHz, with return losses of −30.38 dB, −33.37 dB, and −19.33 dB, respectively. The gains reported are 3.97 dB, 4.34 dB, and 5.66 dB, along with radiation efficiencies of 81.5%, 85%, and 91.2%.

Microstrip patch antennas are commonly used in modern wireless communication systems because of their low profile, lightweight design, and ease of fabrication. These antennas consist of a radiating patch mounted on a dielectric substrate, with a ground plane located beneath. The shape of the patch can vary rectangular, circular, or triangular to meet specific design requirements. Microstrip patch antennas are ideal for applications that require a compact size and planar configuration, such as mobile devices, satellite communication, and radar systems. They typically offer moderate gain and can be easily integrated with planar circuits. However, they are known for having a narrow bandwidth and low power-handling capability. These limitations can be addressed through advanced design techniques, including array configuration, polarization control, and bandwidth optimization, which enhance their overall performance. Based on the advantages and disadvantages of previous designs, this study presents a microstrip patch antenna designed for 6G applications. The antenna has a lightweight and compact structure in a rectangular shape, featuring cut-out insets. The design process involved three different shapes to achieve optimal performance. The main contributions of this work include:

- A compact microstrip antenna that operates at THz dual bands of 147.42 GHz and 202.5 GHz, demonstrating its suitability for implementation in 6G technologies.

- A very low return loss of −44.776 dB at 202.5 GHz, indicating excellent impedance matching.
- The use of response surface methodology (RSM) along with a rotatable central composite design (RCCD) in design-expert to optimize key geometric parameters within the frequency range of 120–220 GHz.
- Simulation setup and verification conducted using computer simulation technology (CST) Studio Suite software, which is widely accepted as an industry standard for high-frequency electromagnetic analysis.
- Achieved gains of 2.66 dB and 4.52 dB for the two frequency bands, with comparisons made to prior studies to establish the design's effectiveness.

The organization of the paper is as follows: section 2 presents the method, calculation of the antenna and the design specifications, while the simulated results are discussed in section 3. Finally, the paper provides the conclusion in section 4.

2. ANTENNA DESIGN METHODOLOGY

The initial shape of the microstrip patch antenna is rectangular, which makes it easy to design. The patch antenna consists of a ground plane, substrate, and patch. The preliminary design of a rectangular microstrip patch antenna operating at 140 GHz, targeted for sub-THz applications such as 6G wireless communications. The design parameters are calculated based on standard transmission-line models, considering a low-permittivity substrate to minimize radiation loss at high frequencies. To accomplish particular goals, researchers frequently choose substrates with a dielectric constant (ε_r) values higher than 2.2. Rogers RO3003 is one such material. The Rogers substrate family offers a range of flexible substrates designed to meet particular microwave construction requirements. These substrates typically consist of a single layer of metallization supporting microstrip construction and may include thick metal backing to enhance mechanical stability and heat dissipation [21]. These substrates provide a low and stable ε_r (approximately 3.0), a very low loss tangent (approximately 10^{-3}), minimal moisture absorption, and excellent thermal stability. These properties help reduce dielectric attenuation and frequency drift, especially in high mmWave/sub-THz frequency ranges. Therefore, the antenna is designed on a Rogers RO3003 substrate (its dielectric constant ε_r is equal to 3, and its coefficient of tangent of dissipation is equal to 0.001, and its thickness h was fixed at 0.1 mm). The design equations that determine the dimensions of the antenna below are referenced in [22].

The maximum value of the substrate height h was determined as:

$$h \leq \frac{0.3c}{2\pi f_0 \sqrt{\varepsilon_r}} \tag{1}$$

where c is the velocity of light ($c = 3.10^8$ m/s), the resonance frequency $f_0 = 140$ GHz, and $\varepsilon_r = 3$. The patch width (W_p) is initially estimated as:

$$W_p = \frac{c}{2f_0}\sqrt{\frac{2}{\varepsilon_r+1}} \tag{2}$$

The effective dielectric constant ε_{eff} is given by:

$$\varepsilon_{eff} = \frac{\varepsilon_r+1}{2} + \frac{\varepsilon_r-1}{2} \cdot \frac{1}{\sqrt{1+\frac{12h}{W_p}}} \tag{3}$$

The effective length (L_{eff}) is calculated from:

$$L_{eff} = \frac{c}{2f_0\sqrt{\varepsilon_{eff}}} \tag{4}$$

The extension of the patch length ΔL is:

$$\Delta L = 0.412h \cdot \frac{(\varepsilon_{eff}+0.3)\left(\frac{W_p}{h}+0.264\right)}{(\varepsilon_{eff}-0.258)\left(\frac{W_p}{h}+0.8\right)} \tag{5}$$

The actual patch length L_p is:

$$L_p = L_{eff} - 2\Delta L \tag{6}$$

Recommended ground plane: extend each side by $\lambda_0/4$.

$$L_g = L_p + 2.\delta$$
$$W_g = W_p + 2.\delta \quad (7)$$

where δ is the edge extension (choose $\delta = \lambda_0/4$) and $\lambda_0 = \frac{c}{f_0}$ (free-space wavelength). Characteristic impedance Z_0.The determination of the auxiliary variables x and y as:

$$x = \frac{Z_0}{60}\left(\frac{\varepsilon_r+1}{2}\right)^{0.5} + \frac{\varepsilon_r-1}{\varepsilon_r+1}\left(0.23 + \frac{0.11}{\varepsilon_r}\right) \quad (8)$$

$$y = \frac{60\pi^2}{Z_0\sqrt{\varepsilon_r}} \quad (9)$$

The dimensions of the power transmission cable can be calculated:

$$W_f = \frac{2h}{\pi}\left[x - 1 - ln(2x-1) + \frac{\varepsilon_r-1}{2\varepsilon_r}\left(ln(x-1) + 0.39 - \frac{0.61}{\varepsilon_r}\right)\right] \quad (10)$$

$$L_f = 3h \quad (11)$$

After determining the parameters using (1)÷(11), the antenna dimensions are then optimized using the RSM as outlined by [23]. We used a RCCD within RSM with four factors: patch length (L_p), patch width (W_p), first inset-slot width (W_1), and second inset-slot width (W_2). These factors were chosen as independent variables to minimize the return loss because they have a substantial influence on the outcome. All other patch-antenna parameters were held constant. The design comprised 29 runs (16 factorial, 8 axials, and 5 center) executed in randomized order. The axial (star) points were set at a distance of $\alpha = 2$ from the center. Optimization targeted minimizing the return loss across the 120 to 220 GHz band using the numerical optimizer in design expert, and was complemented by a graphical optimization window to visualize robust feasible regions, for example, cases in which the return loss does not exceed −44 dB and the operating frequency lies between 120 GHz and 220 GHz. Analysis of variance (ANOVA) indicated significant quadratic models for all responses, with coefficients of determination (R^2) up to 0.97, a non-significant lack of fit, and clearly curved response surfaces with an interior minimum. The numerically predicted optimum $(L_p, W_p, W_1, W_2) = (0.7, 0.7, 0.6, 0.1)$ mm was obtained and validated in CST, confirming stable convergence of the RSM solution. Finally, the optimized antenna dimensions are listed in Table 1.

In this work, Figure 1 illustrates the antenna's progression process in three phases, evaluated through simulation analyses. The recommended design process starts by obtaining three antenna configurations. First, Antenna I features a simple rectangular patch, as shown in Figure 1(a). In the second step, a single rectangular slot is added to the radiating patch, resulting in Antenna II (Figure 1(b)). Finally, the proposed Antenna III is created by adding another rectangular slot to the radiating element, as depicted in Figure 1(c).

Table 1. Antenna parameter values

Parameter	Value (mm)	Parameter	Value (mm)	Parameter	Value (mm)
L_g	1	L_f	0.2	L_2	0.1
W_g	1	W_f	0.08	W_2	0.1
L_p	0.7	L_1	0.2	L_a	0.15
W_p	0.7	W_1	0.6	L_b	0.15

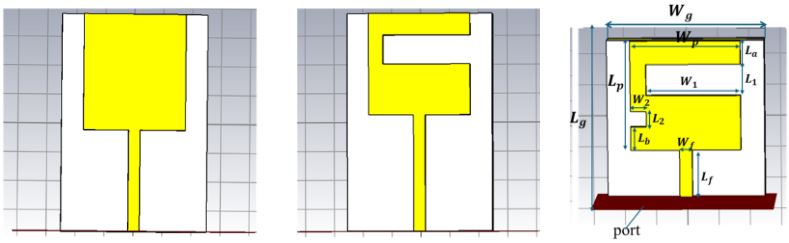

(a) (b) (c)

Figure 1. Progression of antenna design: (a) Antenna I, (b) Antenna II, and (c) Antenna III

3. RESULTS AND DISCUSSION

The simulation results were obtained using CST Studio Suite 2018 with a vacuum background and open boundary conditions on all faces. A 50-Ω waveguide port excited the microstrip feed. Open boundaries, implemented with perfectly matched layer (PML), had an automatic minimum distance of 0.25 λ_0 in all directions at a reference frequency of 170 GHz. The PML target reflection level was set to 10^{-4}, balancing accuracy and computational time for antenna simulations at this band. The frequency-domain solver with a tetrahedral mesh was used, with a frequency range of 120–220 GHz, which automatically selected non-uniform sample points within the band until the desired accuracy was achieved. A time-domain solver with a hexahedral mesh and adaptive mesh refinement (AMR) was also used. The simulation spanned 120–220 GHz, with AMR tuned to S-parameters across the band, using a convergence threshold of 0.01–0.02 (linear) and 3–10 refinement passes. Local mesh controls ensured fine elements around patch edges, inset corners, and the port, with a minimum element size of less than 0.01 mm. Far-field monitors placed at resonance frequencies of 147.42 GHz and 202.5 GHz were used to extract radiation patterns, directivity, and bandwidth. A mesh-independence check involving doubling local refinement showed shifts of less than 0.01 GHz and 0.05 dB. The performance of the microstrip patch antenna is evaluated using various metrics. Key characteristics include return loss, voltage standing wave ratio (VSWR) and radiation gain. These metrics provide information about the antenna's impedance matching, operating frequency range, and signal transmission quality. Analyzing these features contributes to a comprehensive assessment of the microstrip patch antenna's effectiveness in wireless applications, offering a clear understanding of the antenna's overall performance.

3.1. Return loss (S11 parameter)

The return loss (S11) is a reflection coefficient that represents the ratio of the reflected signal power to the incident signal power at the port of a device. S11 is typically expressed in decibels (dB), where lower values indicate better impedance matching and minimal signal reflection. A lower S11 value (e.g., below −10 dB) means better impedance matching and more efficient power transfer. The S11 parameter simulation results for three antennas are shown in Figure 2.

After simulation, Antenna I exhibits a single resonance at 207.3 GHz with a −10 dB bandwidth of 7.04 GHz and a measured reflection coefficient of $S11 = -17.42$ dB. The simulated S11 for Antenna II reveals a dual-band response with resonances at 149.57 GHz and 199.57 GHz. The corresponding return losses and approximate bandwidths are −15.89 dB (4.33 GHz) and −22.023 dB (14.36 GHz), respectively. Comparing these results to Antenna I shows that slotting the patch successfully created additional resonances and substantially improved matching. The simulation of Antenna III indicates small frequency shifts: the lower resonance shifts from 149.57 GHz to 147.42 GHz with improved return loss ($S11 = -19.818$ dB) and the upper resonance shifts from 199.57 GHz to 202.5 GHz with $S11 = -44.776$ dB. These changes demonstrate that the rectangular slotting further refines the matching and slightly tunes the resonance positions.

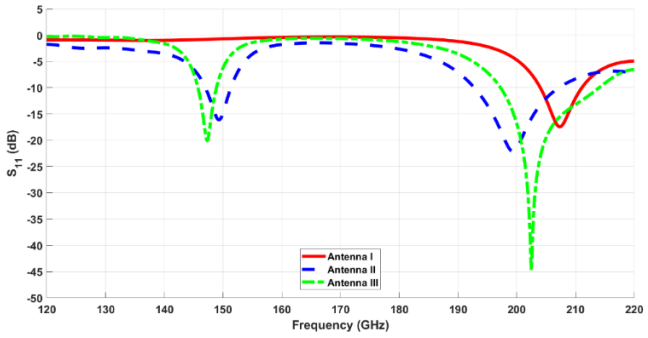

Figure 2. Simulation of the S11 parameter for the development of three antennas

3.2. VSWR

The VSWR of the designed Antenna III is shown in Figure 3. The simulated VSWR curve shows that the VSWR values at two resonant frequencies are both below 2, with a minimum value of 1.01 at 202.5 GHz. This indicates an almost perfect impedance match between the antenna and the feed line. Such near-ideal matching ensures that nearly all incident power is radiated with minimal reflection, maximizing radiation efficiency. This exceptional result highlights the effectiveness of the proposed slotting technique in precisely tuning the antenna impedance for dual-band THz applications.

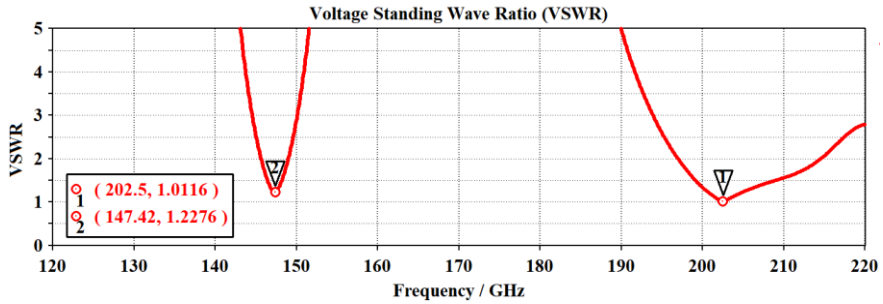

Figure 3. Simulation of the VSWR for the proposed Antenna III

3.3. Gain, radiation pattern, and surface current distribution

Figure 4 presents the simulated three-dimensional (3D) and two-dimensional (2D) radiation patterns of the proposed THz Antenna III. In Figure 4, the results indicate that the recommended antenna achieves maximum gains of 2.66 dB at 147.42 GHz (Figure 4(a)) and 4.52 dB at 202.5 GHz (Figure 4(b)). Figure 5 shows the surface current distribution over the radiating patch, giving insight into the dual-band behavior of the proposed Antenna III with multiple slot geometries.

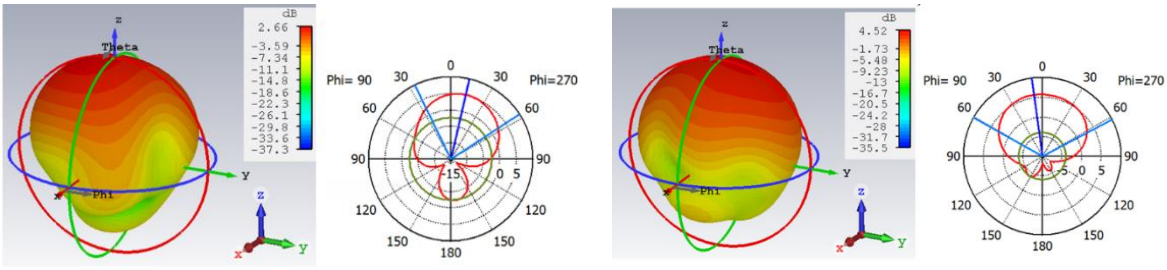

Figure 4. 3D (left) and 2D (right) gain of Antenna III: (a) 147.42 GHz and (b) 202.5 GHz

At the lower frequency band (about 147.42 GHz), as shown in Figure 5(a), currents follow the patch rim and wrap around the long slot with strong concentration at the slot neck. This improves the effective electrical path and creates the first (lower) resonance. At the upper frequency band (approximately 202.5 GHz), as depicted in Figure 5(b), currents are concentrated around the neck and center slot, resulting in a shorter loop that supports the second (higher) resonance. In both cases, the lower ground edge exhibits weak excitation, which indicates that radiation is primarily influenced by the fringing fields at the edges of the patch and slot, rather than by the feed or ground. The long slot and its neck create two coupled resonant paths: one is longer and more inductive, while the other is shorter and more capacitive. This results in dual resonances, which contribute to improvements in return loss, VSWR, gain, and radiation patterns. These enhancements are supported using the proposed slotting geometry across the targeted THz frequency bands.

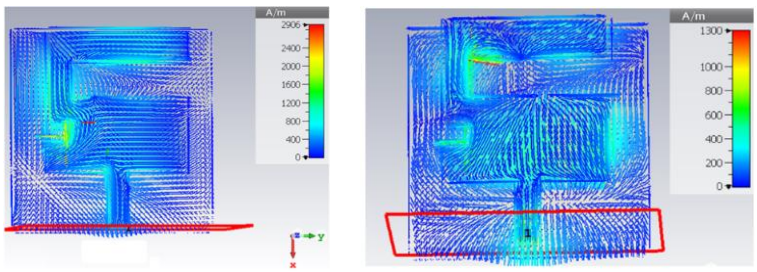

Figure 5. Surface current distribution of Antenna III: (a)147.42 GHz and (b) 202.5 GHz

3.4. Radiation efficiency

The radiation efficiency and total efficiency of the designed antenna are depicted in Figure 6. Figure 6 shows that the antenna achieves a radiation efficiency of 57.5% (–2.4 dB) and 69.2% (–1.6 dB) at the two resonant frequencies. It is clear from Figure 6 that, at both operating frequencies, the total efficiency is nearly the same as the radiation efficiency. There is a key relationship: total efficiency = radiation efficiency × mismatch loss [24]. Therefore, this equality indicates that the mismatch loss is negligible (around 1, or 0 dB), confirming that the design achieves nearly ideal impedance matching. Consequently, the moderate gain values are not due to poor impedance matching but are instead caused by dielectric loss in the substrate and conductor loss in the metal.

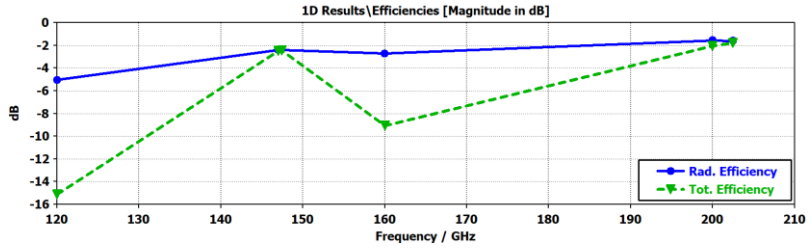

Figure 6. Radiation efficiency (radiation efficiency) and total efficiency (total efficiency) versus frequency (120–220 GHz) for the proposed antenna

3.5. Comparison of the proposed antenna performance with previous works

The comparison of the proposed antenna's characteristics with those previously reported in the literature is shown in Table 2. As shown in Table 2, it attains the lowest S11 value among the compared designs. This result indicates excellent impedance matching. The gains of Antenna III are lower than those reported by [16], [20], [25], but they match or surpass the values in [26]-[28]. While the gains achieved may not be the highest compared to other references, they offer advantages in compact size and integration, particularly with the lowest return loss. As a result, these antennas are suitable for device-to-device communication, wireless connectivity in handheld devices, and THz medical imaging applications. Employing the slotted patch technique enables the antenna to concurrently achieve enhanced return loss, consistent gain, and robust multi-band operation.

Table 2. A comparison of the performance of the designed antenna with that of the existing antenna

Reference/year	Dimensions (mm^3)	Resonant frequency (GHz)	Gain (dB)	S11 (dB)
[20] 2025	1.4×1.1×0.14	123	3.97	−30.38
		168	4.34	−33.37
		182	5.66	−19.33
[25] 2024	1.5×1×0.15	123	4.12	−35.03
		180.4	5.05	−38.71
[26] 2023	0.3×0.3×0.045	362.7–591.8	4	−40
[27] 2022	[0.05-0.09] × [0.05-0.09] × [0.01-0.03]	1000	2.45	−22
[16] 2021	—	4.9	16.950	−33.59
[28] 2021	1.5×1×0.15	1810	1	−17.51
		2640	1.03	−22.08
		4410	1.22	−10.56
This work	1×1×0.1	147.42	2.66	−19.818
		202.5	4.52	−44.776

4. CONCLUSION

The objective of this study was to design a rectangular patch antenna for a 6G communication system that is simple to produce and can be easily integrated into THz systems. To enhance the antenna's performance, a slot technique was employed. Initially, a basic rectangular patch antenna operated at a single frequency of 207.3 GHz. However, after incorporating slots into the patch, the antenna was able to function across two frequency bands at 147.42 GHz and 202.5 GHz, with return losses of −19.818 dB and −44.776 dB, respectively. The recommended dimensions for the antenna are 1 mm × 1 mm × 0.1 mm, achieving gains of 2.66 dB and 4.52 dB. This antenna outperformed several designs in terms of gain and reflection coefficient, making it a strong candidate for 6G wireless applications. The design achieves nearly ideal impedance matching; thus, power loss is governed not by reflection but by dielectric loss in the substrate and conductor

loss in the metal. In future work, we will develop an antenna array based on this patch element to increase overall gain and enable beam steering. In addition, while cross-tool replication in another software package (e.g., high-frequency structure simulator (HFSS)) is beyond the current scope, we plan to port the model and report side-by-side results in follow-up work.

ACKNOWLEDGMENTS

We acknowledge the Vietnam Aviation Academy (VAA) for supporting this study.

FUNDING INFORMATION

Authors state no funding involved.

AUTHOR CONTRIBUTIONS STATEMENT

This journal uses the Contributor Roles Taxonomy (CRediT) to recognize individual author contributions, reduce authorship disputes, and facilitate collaboration.

Name of Author	C	M	So	Va	Fo	I	R	D	O	E	Vi	Su	P	Fu
Bich Ngoc Tran-Thi	✓	✓	✓	✓	✓	✓		✓	✓	✓	✓	✓	✓	
Trong Hai Le			✓			✓		✓	✓	✓				

C : **C**onceptualization
M : **M**ethodology
So : **So**ftware
Va : **Va**lidation
Fo : **Fo**rmal analysis
I : **I**nvestigation
R : **R**esources
D : **D**ata Curation
O : Writing - **O**riginal Draft
E : Writing - Review & **E**diting
Vi : **Vi**sualization
Su : **Su**pervision
P : **P**roject administration
Fu : **Fu**nding acquisition

CONFLICT OF INTEREST STATEMENT

The authors declare that they have no conflict of interest.

DATA AVAILABILITY

The datasets generated and/or analyzed during the current study are available from the corresponding author upon reasonable request.

REFERENCES

[1] J. F. O'Hara, S. Ekin, W. Choi, and I. Song, "A Perspective on Terahertz Next-Generation Wireless Communications," *Technologies*, vol. 7, no. 2, p. 43, Jun. 2019, doi: 10.3390/technologies7020043.
[2] S. P. -Khanjari, F. B. Zarrabi, and S. Jarchi, "Compact and wide-band Quasi Yagi-Uda antenna based on periodic grating ground and coupling method in terahertz regime," *Optik*, vol. 203, p. 163990, Feb. 2020, doi: 10.1016/j.ijleo.2019.163990.
[3] M. Z. Chowdhury, M. Shahjalal, S. Ahmed, and Y. M. Jang, "6G Wireless Communication Systems: Applications, Requirements, Technologies, Challenges, and Research Directions," *IEEE Open Journal of the Communications Society*, vol. 1, pp. 957–975, 2020, doi: 10.1109/OJCOMS.2020.3010270.
[4] Z. R. M. Hajiyat, A. Ismail, A. Sali, and M. N. Hamidon, "Antenna in 6G wireless communication system: Specifications, challenges, and research directions," *Optik*, vol. 231, p. 166415, Apr. 2021, doi: 10.1016/j.ijleo.2021.166415.
[5] A. Youssef, I. Halkhams, R. El Alami, M. O. Jamil, and H. Qjidaa, "A simulation study of dual band THz soft antenna for biomedical applications," *Scientific African*, vol. 25, p. e02294, Sep. 2024, doi: 10.1016/j.sciaf.2024.e02294.
[6] S. Saravanan, K. U. Haimavathi, and K. Aafizaa, "Biomedical Antenna Design: Micro strip Patch Antennas for Wearable and Implantable Healthcare Applications—A Review," *Biomedical Materials and Devices*, vol. 4, no. 1, pp. 414–424, Mar. 2026, doi: 10.1007/s44174-025-00299-0.
[7] P. Hillger, J. Grzyb, R. Jain, and U. R. Pfeiffer, "Terahertz Imaging and Sensing Applications With Silicon-Based Technologies," *IEEE Transactions on Terahertz Science and Technology*, vol. 9, no. 1, pp. 1–19, Jan. 2019, doi: 10.1109/TTHZ.2018.2884852.
[8] M. S. Talukder, M. Samsuzzaman, M. T. Islam, R. Azim, M. Z. Mahmud, and M. T. Islam, "Compact ellipse shaped patch with ground slotted broadband monopole patch antenna for head imaging applications," *Chinese Journal of Physics*, vol. 72, pp. 310–326, Aug. 2021, doi: 10.1016/j.cjph.2021.05.005.
[9] S. Fakhte and M. M. Taskhiri, "Graphene-based terahertz antenna with polarization reconfiguration," *Physica Scripta*, vol. 98, no. 11, p. 115541, Nov. 2023, doi: 10.1088/1402-4896/ad03ca.
[10] F. Yang, X. X. Zhang, X. Ye, and Y. Rahmat-Samii, "Wide-band E-shaped patch antennas for wireless communications," *IEEE Transactions on Antennas and Propagation*, vol. 49, no. 7, pp. 1094–1100, Jul. 2001, doi: 10.1109/8.933489.
[11] G. Singh, K. S. Sandha, and A. Kansal, "GA based optimized graphene antenna design for detection of explosives and drugs using THz spectroscopy," *Micro and Nanostructures*, vol. 179, p. 207566, Jul. 2023, doi: 10.1016/j.micrna.2023.207566.

[12] K. Dave *et al.*, "Graphene-based double-loaded complementary split ring resonator (CSRR) slotted MIMO patch antenna for spectroscopy and imaging THz applications," *Applied Physics A: Materials Science and Processing*, vol. 128, no. 8, p. 656, Aug. 2022, doi: 10.1007/s00339-022-05820-6.
[13] R. Pant and L. Malviya, "THz antennas design, developments, challenges, and applications: A review," *International Journal of Communication Systems*, vol. 36, no. 8, May 2023, doi: 10.1002/dac.5474.
[14] P. Jeyakumar *et al.*, "Broadband complementary ring-resonator based terahertz antenna for 6G application," *Applied Physics A: Materials Science and Processing*, vol. 130, no. 8, p. 604, Aug. 2024, doi: 10.1007/s00339-024-07763-6.
[15] M. Krishna Ch, T. Islam, N. Suguna, S. V. Kumari, R. D. H. Devi, and S. Das, "A micro-scaled graphene-based wideband (0.57–1.02 THz) patch antenna for terahertz applications," *Results in Optics*, vol. 12, p. 100501, Jul. 2023, doi: 10.1016/j.rio.2023.100501.
[16] Y. Shi, X. Zhang, Q. Qiu, Y. Gao, and Z. Huang, "Design of Terahertz Detection Antenna with Fractal Butterfly Structure," *IEEE Access*, vol. 9, pp. 113823–113831, 2021, doi: 10.1109/ACCESS.2021.3103205.
[17] B. Aqlan, M. Himdi, L. L. Coq, and H. Vettikalladi, "Sub-THz Circularly Polarized Horn Antenna Using Wire Electrical Discharge Machining for 6G Wireless Communications," *IEEE Access*, vol. 8, pp. 117245–117252, 2020, doi: 10.1109/ACCESS.2020.3003853.
[18] M. A. Campo, G. Carluccio, D. Blanco, O. Litschke, S. Bruni, and N. Llombart, "Wideband Circularly Polarized Antenna with In-Lens Polarizer for High-Speed Communications," *IEEE Transactions on Antennas and Propagation*, vol. 69, no. 1, pp. 43–54, Jan. 2021, doi: 10.1109/TAP.2020.3008638.
[19] G. B. Wu, Y. S. Zeng, K. F. Chan, S. W. Qu, and C. H. Chan, "High-gain circularly polarized lens antenna for terahertz applications," *IEEE Antennas and Wireless Propagation Letters*, vol. 18, no. 5, pp. 921–925, May 2019, doi: 10.1109/LAWP.2019.2905872.
[20] Y. Amraoui, I. Halkhams, R. El Alami, M. O. Jamil, and H. Qjidaa, "A compact triband patch antenna design at terahertz frequencies," *TELKOMNIKA (Telecommunication Computing Electronics and Control)*, vol. 23, no. 3, p. 588, Jun. 2025, doi: 10.12928/telkomnika.v23i3.26161.
[21] N. B. Kwe, V. Yadav, M. Kumar, S. V. Savilov, M. Z. A. Yahya, and S. K. Singh, "A comparative study of dielectric substrate materials effects on the performance of microstrip patch antenna for 5G/6G application," *Journal of Materials Science: Materials in Electronics*, vol. 35, no. 24, p. 1617, Aug. 2024, doi: 10.1007/s10854-024-13380-z.
[22] S. E. Didi, I. Halkhams, M. Fattah, Y. Balboul, S. mazer, and M. El Bekkali, "Design of a microstrip antenna patch with a rectangular slot for 5G applications operating at 28 GHz," *Telkomnika (Telecommunication Computing Electronics and Control)*, vol. 20, no. 3, pp. 527–536, Jun. 2022, doi: 10.12928/TELKOMNIKA.v20i3.23159.
[23] B. N. Tran-Thi and D. Van Su, "Return Loss Optimization in Rectangular Microstrip Patch Antennas Using Response Surface Methodology (RSM) for 5G Applications," *EAI Endorsed Transactions on Industrial Networks and Intelligent Systems*, vol. 12, no. 3, Jun. 2025, doi: 10.4108/eetinis.v12i3.8948.
[24] C. A. Balanis, *Antenna Theory: Analysis and Design*, 4th ed. John Wiley & Sons, 2016.
[25] A. Youssef, I. Halkhams, R. El Alami, M. O. Jamil, and H. Qjidaa, "Innovative flexible and compact patch antenna for multiband terahertz applications," *Scientific African*, vol. 24, p. e02196, Jun. 2024, doi: 10.1016/j.sciaf.2024.e02196.
[26] S. Kiani, P. Rezaei, and M. Fakhr, "On-chip coronavirus shape antenna for wide band applications in terahertz band," *Journal of Optics (India)*, vol. 52, no. 2, pp. 860–867, Jun. 2023, doi: 10.1007/s12596-022-01048-y.
[27] M. R. Nickpay, M. Danaie, and A. Shahzadi, "Wideband Rectangular Double-Ring Nanoribbon Graphene-Based Antenna for Terahertz Communications," *IETE Journal of Research*, vol. 68, no. 3, pp. 1625–1634, May 2022, doi: 10.1080/03772063.2019.1661801.
[28] G. J. Nissiyah and M. G. Madhan, "Graphene based microstrip antenna for triple and quad band operation at terahertz frequencies," *Optik*, vol. 231, p. 166360, Apr. 2021, doi: 10.1016/j.ijleo.2021.166360.

BIOGRAPHIES OF AUTHORS

Bich Ngoc Tran-Thi was born in Phu Tho Province, Vietnam. She earned her B.S. and M.S. in Physics (Communication Systems) from Southern Federal University (SFU) in Rostov-on-Don, Russia, in 2002 and 2004, respectively. She obtained her Ph.D. from the Faculty of Electrical and Electronics Engineering at Ho Chi Minh City University of Technology in 2024. Currently, she works as a lecturer at the Faculty of Aviation Operations at Vietnam Aviation Academy. Her research interests include antennas, wireless communications, and low-density parity-check decoder architectures on FPGA platforms. She can be contacted at email: ngocttb@vaa.edu.vn.

Trong Hai Le was born in Thanh Hoa Province, Vietnam. He received his B.S. in Air Traffic Management from Vietnam Aviation Academy in 2023. Currently, he works as a teaching assistant at the Faculty of Aviation Operations at Vietnam Aviation Academy. His research interests include wireless communications, flight management and communication, navigation, and surveillance (CNS) technologies. He can be contacted at email: hailt@vaa.edu.vn.